

---

# The GOCE Estimated Moho Beneath the Tibetan Plateau and Himalaya

Daniele Sampietro, Mirko Reguzzoni, and Carla Braitenberg

---

## Abstract

A better understanding of the physics of the Earth's interior is one of the key objectives of the ESA Earth Explorer missions. This work is focused on the GOCE mission and presents a numerical experiment for the Moho estimation under the Tibet-Quinghai Plateau and the Himalayan range by exploiting the gravity data collected by this mission. The gravity observations, at satellite level, are first reduced for the topography, oceans and known sediments and then the residual field is inverted to determine the crust–mantle interface. The uniqueness of the solution is guaranteed using this simplified two-layer model by making assumptions on the density contrast. Our inversion algorithm is based on the linearization of the Newton's gravitational law around an approximate constant Moho depth. The resulting equations are inverted by exploiting the Wiener–Kolmogorov theory in the frequency domain and treating the Moho depth as a random signal with zero mean and its own covariance function. As for the input gravity observations, we considered grids of the anomalous gravitational potential and its second radial derivative at satellite altitude, as computed by applying the so called space-wise approach to 8 months of GOCE data. Errors of these grids are available by means of Monte Carlo simulations. Taking a lateral density variations for granted, the Moho beneath the Tibetan Plateau and Himalaya is computed on a grid covering the whole area with an accuracy of few kilometers and an estimated resolution of about 250 km. Taking into account this resolution, the estimated Moho generally shows a good agreement with existing local seismic profiles. The areas where this agreement is not so good can be clearly attributed to the presence of anomalies in the crust–mantle separation, such as subduction zones. The GOCE-only solution is finally improved by using seismic profiles as additional observations, locally increasing its accuracy and resolution.

---

## Keywords

GOCE mission • Moho • Tibet • Himalaya • Earth's gravity field • Earth's interior • Inverse gravimetric problem

---

D. Sampietro (✉)  
DIIAR, Politecnico di Milano, Polo Territoriale di Como,  
Via Valleggio 11, 22100 Como, Italy  
e-mail: [daniele.sampietro@polimi.it](mailto:daniele.sampietro@polimi.it)

M. Reguzzoni  
DIIAR, Politecnico di Milano, Piazza Leonardo da Vinci 32, 20133  
Milano, Italy  
e-mail: [mirko@geomatica.como.polimi.it](mailto:mirko@geomatica.como.polimi.it)

C. Rizos and P. Willis (eds.), *Earth on the Edge: Science for a Sustainable Planet*, International Association of Geodesy Symposia 139, DOI 10.1007/978-3-642-37222-3\_52,  
© Springer-Verlag Berlin Heidelberg 2014

---

## 1 Introduction

Numerous geophysical studies faced the problem of recovering the shape of the Moho beneath the Tibetan Plateau and the Himalayas: in particular the crustal structure

---

C. Braitenberg  
Department of Mathematics and Geosciences, University of Trieste,  
Piazzale Europa 1, 34127 Trieste, Italy  
e-mail: [berg@units.it](mailto:berg@units.it)

was investigated by several seismic exploration campaigns (e.g., Kind et al. 2002; Haines et al. 2003; Zhang and Klemperer 2005; Tseng et al. 2009), from studies based on gravimetric inversion (e.g., Braitenberg et al. 2000a,b) and from flexural models (e.g., Jin et al. 1996; Caporali 2000; Braitenberg et al. 2003). However all these models, based on seismic or gravity ground data, are inevitably limited in the Tibetan Plateau and the Himalayas by the poor data coverage due to the extreme topography of those regions.

The idea to overcome this geographical limitation by exploiting gravitational information coming from satellite missions (e.g. GRACE) has recently been proposed by Shin et al. (2007) and improved by Shin et al. (2009). However, due to the smoothing effect of the altitude on the gravitational field, the inversion has never been performed directly from satellite observations but it has been done from global gravity model that mixed up ground gravity anomalies with satellite data. The recent release of GOCE data (Floberghagen et al. 2011), one of ESA Earth Explorer missions, allows for the first time to directly invert a large amount of gravitational observations acquired in a uniform mode with high accuracy and resolution (1–2 mgal accuracy at about 100 km resolution in terms of ground gravity anomalies).

In this framework, we present a new 3D Moho model beneath the Tibetan Plateau and the Himalayan region obtained from a direct inversion of GOCE gravimetric observations. In order to guarantee the uniqueness of the solution a two-layer model is assumed. Although the actual crust–mantle boundary can be locally much more complicated than this simplified model, for instance showing doubling, fragmentation or a broad transition, as documented in the provided references and in many other publications, the resulting Moho is found to be generally consistent with existing models (e.g. with the profiles shown in Zhang and Klemperer 2005; Tseng et al. 2009). Among other things, this research represents a first case study to assess the inversion algorithm based on the linearization of the Newton's gravitational law and to understand the possibility to improve our knowledge of the Moho discontinuity by exploiting GOCE observations (Reguzzoni and Sampietro 2012).

## 2 Gravity Inversion Methodology

The inversion algorithm applied in this work is based on the linearization of the equations of the gravitational potential and its second radial derivative. We recall here the main concepts: considering a spherical coordinate system  $(\varphi, \lambda, r)$ , the gravitational potential  $T$  observed at point P (e.g. at satellite altitude) due to the masses between the Moho and topography can be written as:

$$T(\mathbf{P}) = \iint_S \int_{H_Q}^{M_Q} \frac{G \rho_C r_P^2 \cos \varphi_Q d\varphi_Q d\lambda_Q dr_Q}{l_{PQ}} \quad (1)$$

where  $l_{PQ} = \sqrt{r_P^2 + r_Q^2 + 2r_P r_Q \cos \psi_{PQ}}$  is the distance between points P and Q with  $\psi_{PQ}$  the solid angle between them,  $G$  is the gravitational constant,  $\rho_C$  is the crust density,  $S$  is the surface of the considered region,  $H_Q$  and  $M_Q$  are respectively the radial coordinates of the topography and of the Moho for the point Q. Linearizing Eq. (1) with respect to  $r_Q$  around an a-priori value of the mean Moho depth  $\bar{R}$  and assuming a two-layer hypothesis for the crust–mantle interface, we obtain:

$$T(\mathbf{P}) = \iint_S \int_{H_Q}^{\bar{R}} \frac{G \rho_C r_P^2 \cos \varphi_Q d\varphi_Q d\lambda_Q dr_Q}{l_{PQ}} + \iint_S \frac{G r_P^2 \Delta\rho_Q \delta D_Q \cos \varphi_Q d\varphi_Q d\lambda_Q}{\bar{l}_{PQ}} \quad (2)$$

where  $\bar{l}_{PQ} = \sqrt{r_P^2 + \bar{R}^2 + 2r_P \bar{R} \cos \psi_{PQ}}$ ,  $\delta D_Q$  is the difference between the unknown actual depth of the Moho and the mean Moho depth  $\bar{R}$  at point Q,  $\Delta\rho_Q$  is the density contrast between crust and mantle, i.e.  $\rho_C - \rho_M$  (where  $\rho_M$  is the mantle density) if the actual Moho is deeper than  $\bar{R}$  and  $\rho_M - \rho_C$  if the actual Moho is shallower than  $\bar{R}$ . Note that since all terms in the first integral of Eq. (2) are known, it can be numerically evaluated and subtracted from the original potential obtaining:

$$\delta T(\mathbf{P}) = \iint_S \frac{G r_P^2 \Delta\rho_Q \delta D_Q \cos \varphi_Q d\varphi_Q d\lambda_Q}{\bar{l}_{PQ}}. \quad (3)$$

An analogous reasoning can be applied to the second radial derivative of the gravitational potential:

$$\delta T_{rr}(\mathbf{P}) = \iint_S \frac{\left(3r_P^2 \cos^2 \psi_{PQ} + 4\bar{R}r_P \cos \psi_{PQ} + 2\bar{R}^2 - r_P^2\right)}{\left(r_P^2 + \bar{R}^2 + 2r_P \bar{R} \cos \psi_{PQ}\right)^{\frac{5}{2}}} \cdot \bar{R}^2 G \Delta\rho_Q \delta D_Q \cos \varphi_Q d\varphi_Q d\lambda_Q. \quad (4)$$

If some simplifications are introduced into the problem, i.e. considering  $\xi = \bar{R}\lambda \cos \bar{\varphi}$  and  $\eta = \bar{R}\varphi$  instead of  $\lambda$  and  $\varphi$ , where  $\bar{\varphi}$  is the mean latitude of the considered region, Eqs. (3) and (4) can be rewritten as:

$$\delta T(P) = \iint_S \frac{\frac{\cos \varphi_Q}{\cos \varphi} G \Delta \rho_Q \delta D_Q d\xi_Q d\eta_Q}{\left[ (r_P - \bar{R})^2 + \frac{r_P}{\bar{R}} \sigma_{PQ}^2 \right]^{\frac{1}{2}}} \quad (5)$$

$$\delta T_{rr}(P) = \iint_S \frac{\left[ 3\sigma_{PQ}^4 + 4\bar{R}\sigma_{PQ}^2 (2r_P - 3\bar{R}) + 8\bar{R}^2 (r_P - \bar{R})^2 \right]}{4\bar{R}^2 \left[ (r_P - \bar{R})^2 + \frac{r_P}{\bar{R}} \sigma_{PQ}^2 \right]^{\frac{5}{2}}} \cdot \frac{\cos \varphi_Q}{\cos \varphi} G \Delta \rho_Q \delta D_Q d\xi_Q d\eta_Q \quad (6)$$

where  $\sigma_{PQ} = \sqrt{(\xi_P - \xi_Q)^2 + (\eta_P - \eta_Q)^2}$  is the distance between P and Q in the new Cartesian coordinates  $\xi, \eta$ . If points P are at a constant altitude (i.e.  $r_P = \text{const}$ ) Eqs. (5) and (6) can be expressed as convolution integrals:

$$\delta T(P) = \iint_S k_T(\sigma_{PQ}) \Delta \rho_Q \delta D_Q \cos \varphi_Q d\xi_Q d\eta_Q \quad (7)$$

$$\delta T_{rr}(P) = \iint_S k_{T_{rr}}(\sigma_{PQ}) \Delta \rho_Q \delta D_Q \cos \varphi_Q d\xi_Q d\eta_Q \quad (8)$$

where  $k_T$  and  $k_{T_{rr}}$  are the convolution kernels depending only on the distance  $\sigma_{PQ}$ . Moreover if we also assume that observations are sampled on a regular grid (in  $\xi, \eta$ ) and the Moho is estimated on the same grid points, the system of Eqs. (7) and (8) can be efficiently inverted in terms of Multiple Input Single Output (MISO) Wiener filter in the frequency domain (Papoulis 1965; Sideris and Tziavos 1988; Reguzzoni and Sampietro 2012). Note that here the inversion is not applied in a planar approximation, but in an almost spherical one with respect to the coordinates  $\xi$  and  $\eta$ , thus giving the possibility to consider larger areas, say with an extension up to  $40^\circ$  (Sampietro 2011). We also would like to stress that the proposed inversion method is not able to estimate the mean Moho depth which is taken from external sources. In particular it is here computed by averaging the Moho depth of the CRUST 2.0 model (Bassin et al. 2000) over the considered area, resulting into  $\bar{R} = 40.5$  km. Since this value is also used for the linearization of Eq. (2), a sensitivity analysis has been performed showing that a variation of  $\bar{R}$  by  $\pm 10$  km produces a variation of the estimated  $\delta D$  by about  $\pm 0.6$  km in terms of standard deviation.

In this study two grids, one of the gravitational potential and one of its second radial derivatives, have been used as input for the inversion. These grids are not synthesized by any GOCE global gravity model, but are directly estimated at mean satellite altitude from 8 months of GOCE observations as by-products of the so called space-wise approach (Reguzzoni and Tselfes 2009; Migliaccio et al. 2011). This is

a multi-step collocation procedure, developed in the framework of the GOCE HPF (High Processing Facility, Rummel et al. 2004) data processing for the estimation of the spherical harmonic coefficients of the Earth's gravitational field.

In order to apply our inversion algorithm some power spectral densities (PSDs), or the corresponding covariance functions, are required: we need the PSD of  $\delta D_Q$ , i.e. the PSD of the discontinuity surface between crust and mantle, and the two PSDs of the observation errors. The first can be derived from an a-priori Moho: in particular the theoretical covariance function of the discontinuity surface, modeled as the product of two Gaussian functions in  $\xi, \eta$ , has been computed by least squares fitting an empirical anisotropic covariance obtained from the a-priori Moho. In this study the CRUST 2.0 model is used to derive the a-priori Moho, after smoothing it by means of a moving average to avoid that the very sharp boundaries between the  $2^\circ \times 2^\circ$  cells, especially in the Himalayas, wrongly influence the covariance estimation. For details on the theoretical covariance function used and its fitting to the empirical covariance function we refer to Wackernagel (1995). As for the error spectra of GOCE gridded observations, they are estimated from Monte Carlo samples (Migliaccio et al. 2009).

Additional information has been added to the study. Firstly the effect of sediments in terms of GOCE observables at satellite altitude has been computed by point-mass numerical integration and then removed from the GOCE grids. At global level sediment information is taken from CRUST 2.0, while at local level a more refined sediment model (Braitenberg et al. 2003) is used. Although CRUST 2.0 is quite rough, this global information is necessary because, at satellite level, the gravitational signal over the study area partly depends on the crustal mass distribution all over the world. Note that if sediment density variations were not considered, i.e. they were not used for the evaluation of the first integral in Eq.(2), then their gravitational effect would be wrongly transformed into Moho depth from the inversion algorithm which is based on a two-layer hypothesis. Secondly, lateral variations of density contrast (again from CRUST 2.0) have been taken into account in the inversion keeping the uniqueness of the solution. To this aim one can estimate the product between the Moho depth  $\delta D_Q$  and the point-wise density contrast  $\Delta \rho_Q$ , see Eqs. (7) and (8), and then derive the former by assuming the latter as known (Barzaghi and Sansó 1988; Sampietro and Sansó 2012). Finally two seismic profiles (Fig. 1) have been considered as observations of Moho depth with an error standard deviation of 4.9 km. For a detailed description of the algorithm used to add point-wise ground observations into the inversion procedure we refer to Reguzzoni and Sampietro (2012).

**Fig. 1** Seismic profiles (A-A1 and B-B1) used in the Tibetan region (Zhang and Klemperer 2005; Tseng et al. 2009)

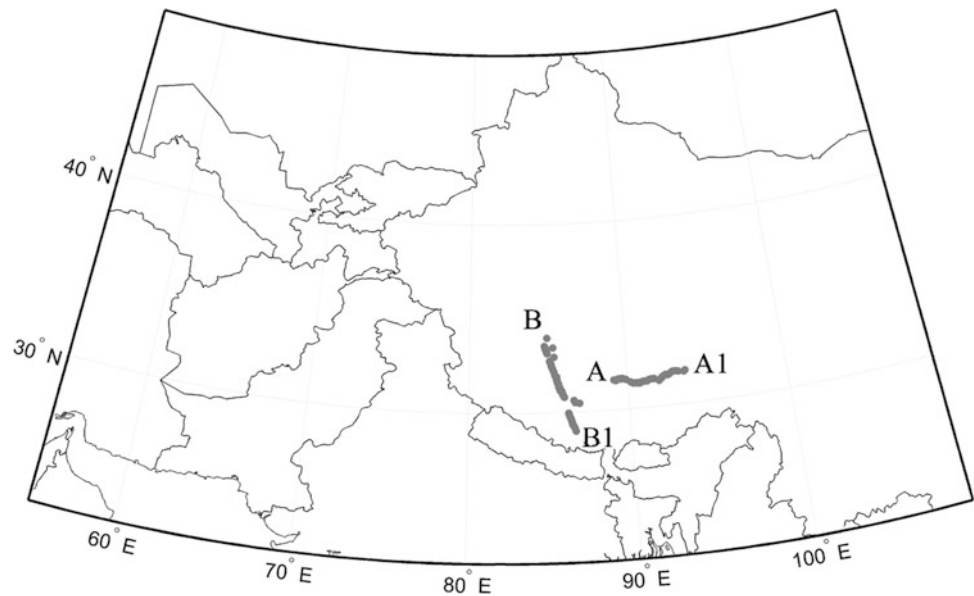
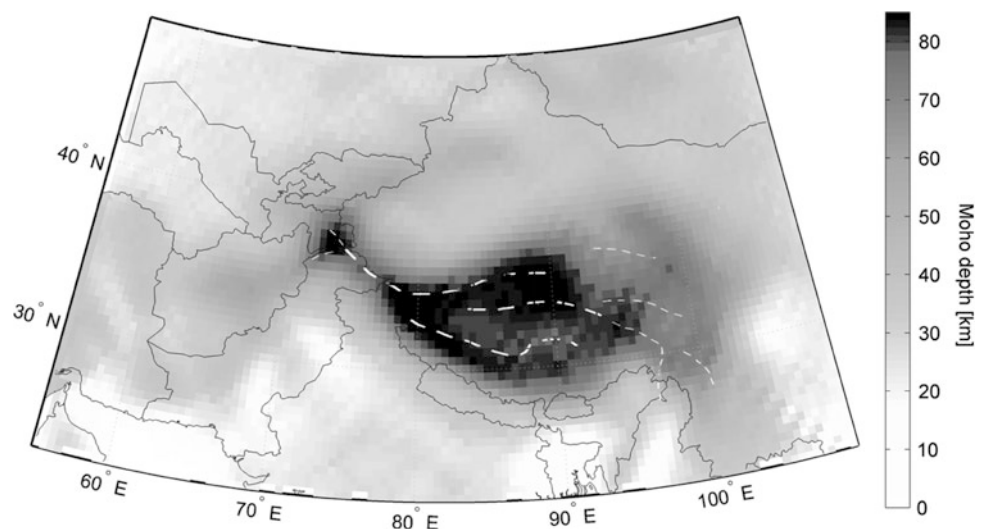


**Fig. 2** Moho estimated inverting GOCE observations only. White dash lines represent the main suture lines



### 3 Results

The Moho depth has been estimated both inverting GOCE-only data and integrating the seismic profiles with GOCE observations (Figs. 2 and 3). In the first case the error covariance function of the estimated model (Fig. 4) has been predicted by propagating the Monte Carlo error covariance matrix of GOCE grids to the results, after approximating it with a Toeplitz–Toeplitz structure (Grenander and Szegő 1958; Reguzzoni and Sampietro 2012). This error covariance function provides information on the model accuracy. Its resolution can be instead inferred by comparing the estimated Moho PSD with the error one (Fig. 5); the minimum resolvable wavelength corresponds to the spatial frequency at which signal and error PSDs are the same, that is about 250 km.

The estimated GOCE-only Moho model has been compared with the available Moho profiles computed from seismic observations (Fig. 6). Recall that the seismic lines contain higher frequency components than the ones we can recover from the inversion of GOCE data. In this sense results seem to be satisfactory because our inversion Moho well interpolates the seismic one, especially for the profile A-A1, while for the profile B-B1 an explanation of the worse agreement is given afterwards.

In addition, while for the signal the correlation is practically zero for spherical distances larger than  $25^\circ$ , for the estimated error (obtained by propagating the error from GOCE observations to the results) this happens roughly above  $2.5^\circ$  (Fig. 4). This error correlation estimate is confirmed by the residuals with the seismic profiles (Fig. 6) showing an empirical covariance function going to zero above  $2^\circ$ . On the contrary the estimated error standard

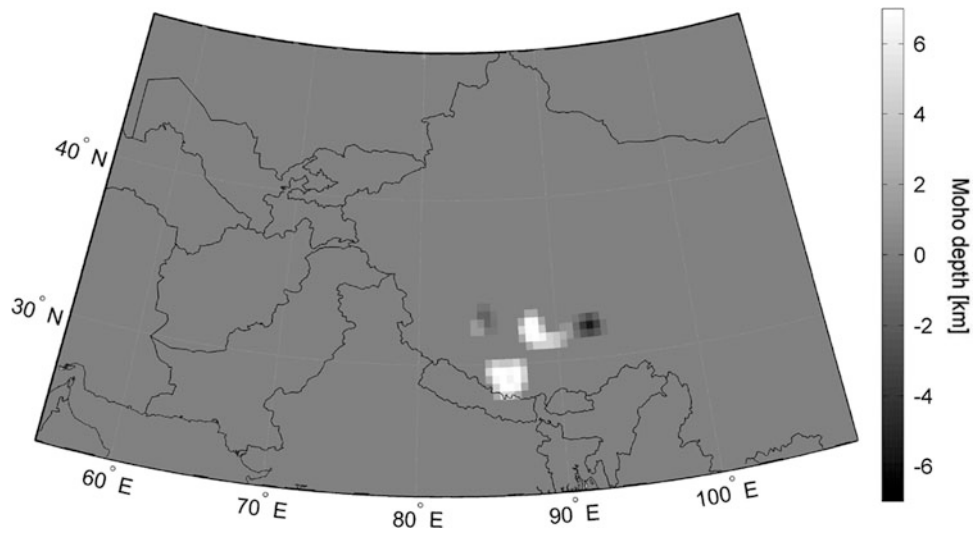


**Fig. 3** Corrections to the GOCE-only Moho due to the integration of the seismic profiles

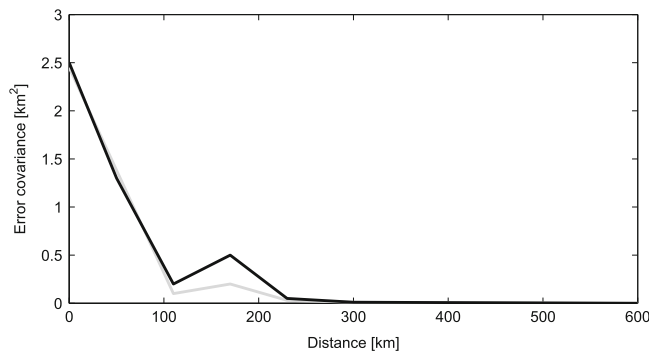


**Fig. 4** Error covariance functions of the estimated GOCE-only Moho in the  $\xi$  (black line) and  $\eta$  (grey line) directions

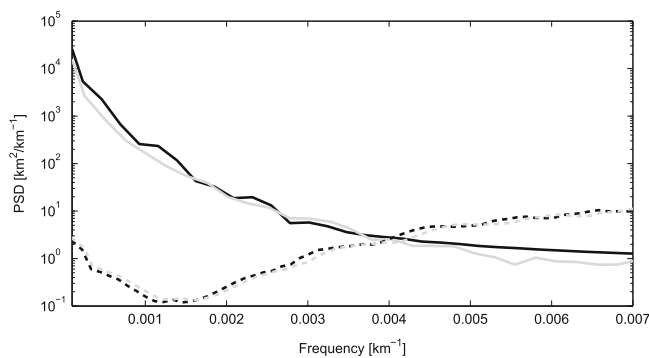


**Fig. 5** Power spectral densities of the estimated GOCE-only Moho (solid lines) and of its error (dash lines), computed along the  $\xi$  (black lines) and  $\eta$  (grey lines) directions

deviation, of the order of 1.6 km (Fig. 4), is much smaller than the one obtained from the residuals with seismic profiles (5 km). This difference is mainly due to the simplified two-layer hypothesis introducing model errors that are not

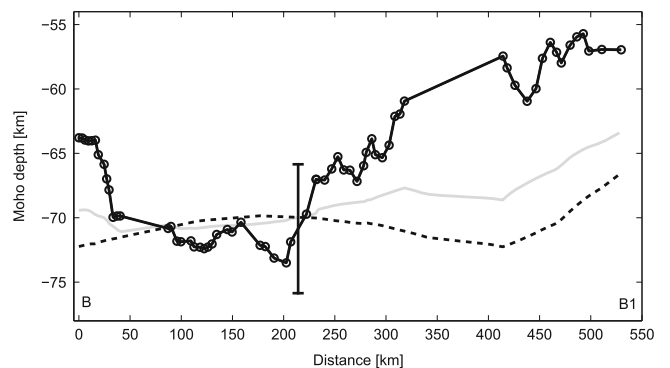
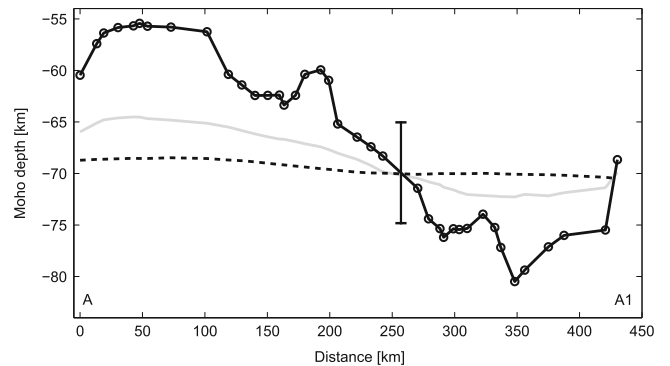


**Fig. 6** Moho models from seismic profiles with their estimated uncertainty (black solid line, observations represented by circles), compared with the GOCE-only Moho (dash line) and the GOCE + seismic Moho (grey line)

accounted for in the estimated Moho error. As already written, CRUST 2.0 information has been used to mitigate this effect; however this global model is quite crude and may contain errors in sediments and density anomalies that are only partially corrected by the used local models of

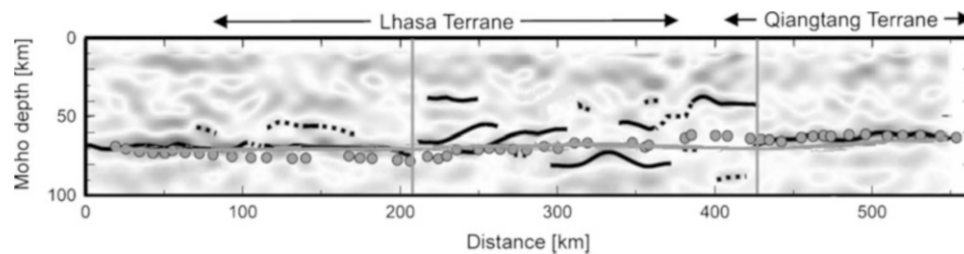


**Fig. 7** Seismic interpretation of the B-B1 profile according to Tseng et al. (2009). Black curves (dashed when uncertain) highlight particularly strong impedance contrasts interpreted as the Moho transition

sediments. A sensitivity analysis has been carried out by separately changing the CRUST 2.0 thickness of sediments and density contrast between crust and mantle up to 50%. Results show that a variation of the sediment thickness of 50% will explain a difference in the Moho estimation of the order of 3 km. The same Moho difference is also produced by an analogous variation in the crust–mantle density contrast.

We can conclude that the intrinsic error of GOCE observations should allow, in principle, to recover the Moho with an accuracy of 1.6 km or better (in terms of standard deviation). However also the combined errors in sediment thickness and density contrast propagate to the estimated Moho model, thus producing an overall degradation of its accuracy down to about 4.5 km (in terms of standard deviation, assuming that each error source is independent of each other). This partially explains the difference obtained between the gravimetric Moho and the seismic profiles, especially in the case of the first profile (A-A1).

As for the Moho model obtained integrating GOCE data and seismic profiles we can note that the mean depth of the Moho is practically unchanged (Fig. 3), while the standard deviation of the residuals with respect to the two seismic profiles decreases to 4 km. This value is not reduced more, as one may expect, because GOCE contribution is overweighed in the combination by collocation (recall the underestimate of the error in the GOCE-only Moho). Moreover the model resolution is locally increased as one can easily notice from Fig. 6.

In the first 200 km of the second profile (B-B1) there is a good agreement between the estimated GOCE-only model and seismic observations, while approximately in the range between 200 and 450 km from the origin the behaviour of two models is visibly different with large discrepancies up to 15 km (Fig. 5). These differences, which are only slightly reduced by integrating the seismic profiles into the estimated model, are in correspondence with the collision between Indian and Eurasian plates where doubling as well as fragmentation of the Moho are present (Fig. 7). Therefore the discrepancy can be explained as a consequence of the fact that the two layer hypothesis is not an acceptable

zone by the authors. Dots display the isostatic Moho. Grey curve is the estimated GOCE-only Moho

approximation in those critical regions. A full model should comprise the subduction of the Indian lithosphere and density variations at lower crustal level across the strike of the Himalayan belt. On the other hand, this numerical result shows that, in principle, discrepancies between GOCE Moho model and seismic profiles can be used to detect the presence of such kind of density anomalies by simply mapping the largest residuals.

All in all, we can conclude that GOCE observations allow to recover all main features of the considered Moho with a wavelength larger than 250 km. Nevertheless it is worth remembering that in the region under study we are dealing with the deepest Moho of the world (with a mean depth of about 40 km and a maximum of over 80 km), so even better results are expected in other regions of the world where the distance between the source of the gravitational signal (Moho surface) and the observation point (GOCE orbit) is smaller, see e.g. Braitenberg et al. (2010).

## 4 Conclusions and Final Remarks

In this paper, GOCE gridded data coming from the space-wise approach have been used to estimate the Moho depth beneath the Tibetan Plateau and the Himalayas (Fig. 2). Crossing Tibet along the East-West direction, GOCE observes a Moho with a small trend parallel to the plateau border and suture lines, while in the North-South direction the presence of an undulation and in particular of three deep Moho belts of some kilometers amplitude is observed. The Moho is in general very deep (more than 70 km) in western and central Tibet with a maximum depth of more than 82 km at 80°E–35°N where the three Moho belts seem to converge. A more superficial Moho, around 65 km depth, is found in eastern Tibet.

These features seem to confirm what already stated in literature (see references in Sect. 1) and also permit to overcome one of the main criticism of the estimation of the Moho from satellite data. In fact, the principal wavelength of the Moho in the considered region is between 330 and 375 km (Shin et al. 2009), which is very close to the shortest

wavelength well recovered by a GRACE-only spherical harmonic development (degree and order 120, about 330 km) but is far above the resolution of GOCE which is able to reconstruct the Moho signal with sufficient accuracy for all wavelengths longer than 250 km, as it is numerically proved in this paper.

The use of seismic observations as additional data (Fig. 3) helps to further increase resolution in the local areas where these observations are available and can mitigate mismodelling effects due to the simplified two layer hypothesis. Moreover, a comparison between GOCE-only Moho and seismic profiles can help to detect areas where the crust–mantle separation shows anomalous behaviours.

**Acknowledgements** This research has been supported by ESA through the STSE program (4000102372/10/I-AM GEMMA project) and by ASI through the GOCE-Italy project.

## References

- Barzaghi R, Sansó F (1988) Remarks on the inverse gravimetric problem. *Geophys J* 92:505–511
- Bassin C, Laske G, Masters G (2000) The current limits of resolution for surface wave tomography in North America. *EOS Trans AGU* 81:F897
- Braitenberg C, Zadro M, Fang J, Wang W, Hsu HT (2000a) Gravity inversion in Qinghai-Tibet Plateau. *Phys Chem Earth* 25:381–386
- Braitenberg C, Zadro M, Fang J, Wang Y, Hsu HT (2000b) The gravity and isostatic Moho undulations in Qinghai-Tibet Plateau. *J Geodyn* 30:489–505
- Braitenberg C, Wang Y, Fang J, Hsu HY (2003) Spatial variations of flexure parameters over the Tibet-Qinghai Plateau. *Earth Planet Sci Lett* 205:211–224
- Braitenberg C, Mariani P, Reguzzoni M, Ussami N (2010) GOCE observations for detecting unknown tectonic features. In: *Proceedings of the ESA living planet symposium, 28 June–2 July 2010, Bergen, Norway*, ESA SP-686
- Caporali A (2000) Buckling of the lithosphere in western Himalaya: constraints from gravity and topography data. *J Geophys Res* 105:3103–3113
- Floberghagen R, Fehring M, Lamarre D, Muzi D, Frommknecht B, Steiger C, Piñeiro J, da Costa A (2011) Mission design, operation and exploitation of the gravity field and steady-state ocean circulation explorer mission. *J Geodesy* 85(11):749–758
- Grenander U, Szegö G (1958) *Toeplitz forms and their applications*. University of California Press, Berkeley
- Haines SS, Klemperer SL, Brown L, Guo J, Mechie J, Meissner R, Ross A, Zhao W (2003) INDEPTH III seismic data: from surface observations to deep crustal processes in Tibet. *Tectonics* 22(1):1001. doi:10.1029/2001TC001305
- Jin Y, McNutt MK, Zhu Y (1996) Mapping the descent of Indian and Eurasian plates beneath the Tibetan Plateau from gravity anomalies. *J Geophys Res* 101:11275–11290
- Kind R, Yuan X, Saul J, Nelson D, Sobolev SV, Mechie J, Zhao W, Kosarev G, Ni J, Achauer U, Jiang M (2002) Seismic images of crust and upper mantle beneath Tibet: evidence for Eurasian plate subduction. *Science* 298:1219–1221
- Migliaccio F, Reguzzoni M, Sansó F, Tselles N (2009) An error model for the GOCE space-wise solution by Monte Carlo methods. In: Sideris MG (ed) *International Association of Geodesy symposia, Observing our changing Earth*, vol 133, pp 337–344
- Migliaccio F, Reguzzoni M, Gatti A, Sansó F, Hecceg M (2011) A GOCE-only global gravity field model by the space-wise approach. In: *Proceedings of the 4th international GOCE user workshop, 31 March–1 April 2011, Munich, Germany*, ESA SP-696
- Papoulis A (1965) *Probability, random variables, and stochastic processes*. McGraw Hill, New York
- Reguzzoni M, Sampietro D (2012) Moho estimation using GOCE data: a numerical simulation. In: Kenyon SC, Pacino MC, Marti U (eds) *International Association of Geodesy symposia, Geodesy for planet Earth*, vol 136, pp 205–214
- Reguzzoni M, Tselles N (2009) Optimal multi-step collocation: application to the space-wise approach for GOCE data analysis. *J Geodesy* 83(1):13–29
- Rummel R, Gruber T, Koop R (2004) High level processing facility for GOCE: products and processing strategy. In: *Proceedings of the 2nd international GOCE user workshop, 8–10 March 2004, Frascati, Rome, Italy*, ESA SP-569
- Sampietro D (2011) GOCE exploitation for moho modeling and applications. In: *Proceedings of the 4th international GOCE user workshop, 31 March–1 April 2011, Munich, Germany*, ESA SP-696
- Sampietro D, Sansó F (2012) Uniqueness theorems for inverse gravimetric problems. In: Sneeuw N, Novák P, Crespi M, Sansó F (eds) *International Association of Geodesy symposia, VII Hotine-Marussi symposium on mathematical geodesy*, vol 137, pp 111–117
- Shin YH, Xu H, Braitenberg C, Fang J, Wang Y (2007) Moho undulations beneath Tibet from GRACE-integrated gravity data. *Geophys J Int* 170:971–985
- Shin YH, Shum C-K, Braitenberg C, Lee SM, Xu H, Choi KS, Baek JH, Park JU (2009) Three-dimensional fold structure of the Tibetan Moho from GRACE gravity data. *Geophys Res Lett* 36:L01302. doi:10.1029/2008GL036068
- Sideris MG, Tziavos IN (1988) FFT-evaluation and applications of gravity-field convolution integrals with mean and point data. *J Geodesy* 62(4):521–540
- Tseng TL, Chen WP, Nowack RL (2009) Northward thinning of Tibetan crust revealed by virtual seismic profiles. *Geophys Res Lett* 36:L24304. doi:10.1029/2009GL040457
- Wackernagel H (1995) *Multivariate geostatistics: an introduction with applications*. Springer, New York
- Zhang Z, Klemperer SL (2005) West-east variation in crustal thickness in northern Lhasa block, central Tibet, from deep seismic sounding data. *J Geophys Res* 110:B09403. doi:10.1029/2004JB003139